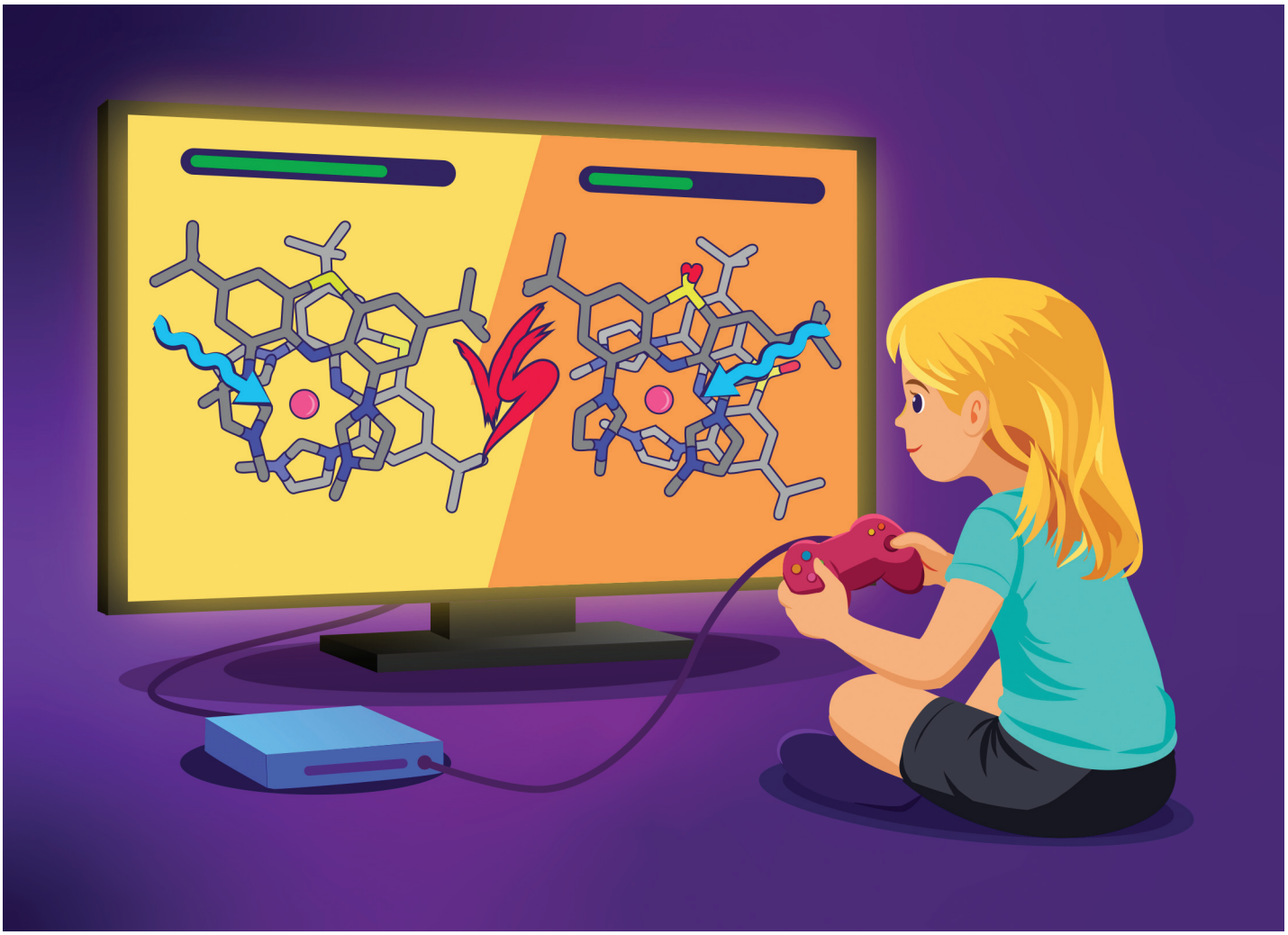

Showcasing research from Professor Michael O. Wolf's laboratory, Department of Chemistry, The University of British Columbia, Vancouver, BC, Canada.

Photophysical properties of Co(III) photosensitizers with phenothiazine-based ligands

This work demonstrates the ability to control the photophysical properties of cobalt(III) photosensitizers using phenothiazine-based ligands. The sulfur oxidation state dictates the metal electronic density and excited-state dynamics.

Image reproduced by permission of Michael O. Wolf from *Inorg. Chem. Front.*, 2026, **13**, 2337.

As featured in:

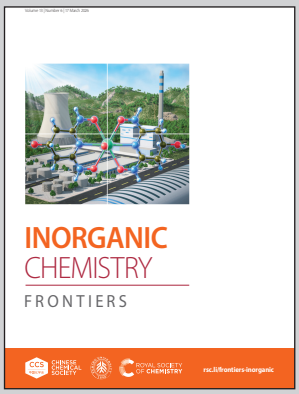

See Michael O. Wolf *et al.*, *Inorg. Chem. Front.*, 2026, **13**, 2337.

INORGANIC CHEMISTRY FRONTIERS

RESEARCH ARTICLE

View Article Online
View Journal | View Issue

Cite this: *Inorg. Chem. Front.*, 2026, **13**, 2337

Photophysical properties of Co(III) photosensitizers with phenothiazine-based ligands

Jessica Toigo, [a] Ka-Ming Tong, [a] Saeid Kamal, [a] Charles J. Walsby, [b] Brian O. Patrick[a] and Michael O. Wolf *[a]

The ultrafast decay inherent to metal complexes with a $3d^6$ configuration limits their application as photosensitizers. Despite recent advances in improving the photophysical properties of these complexes, existing ligand designs restrict further modification and are often synthetically challenging. Here, we show how sulfur-bridged ligands can be used to tune the structural and photophysical properties in Co(III) photosensitizers. Two complexes, **CoS** ($[Co(PTZIm_2)_2]PF_6$) and **$CoSO_2$** ($[Co(PTZO_2Im_2)_2]PF_6$), adopt facial geometries due to a less rigid ligand backbone compared to other pincer-type ligands. The lowest-lying absorption bands of both **CoS** and **$CoSO_2$** display metal/ligand-to-ligand charge-transfer (M + L)LCT character with different contributions from the sulfur-bridged ligand. TD-DFT analysis indicates that **$CoSO_2$** has a lower contribution from the phenothiazine moiety to the band at 400 nm. The sulfur oxidation state also affects the electronic density at the metal center, with **CoS** showing a lower $M^{IV/III}$ oxidation potential. Transient absorption experiments reveal that fast non-radiative decay channels are facilitated in **CoS**. However, a photoactive long-lived component (8.0 ns) is also observed. Oxidation of phenothiazine extends the lifetimes of short-lived components in **$CoSO_2$**, where both electronic and structural effects may be playing a role. These findings demonstrate that the photophysical properties of Co(III) complexes can be modulated by variation of the sulfur oxidation state to achieve different photophysical properties of the complexes.

Received 20th November 2025,
Accepted 6th January 2026

DOI: 10.1039/d5qi02362a

rsc.li/frontiers-inorganic

Introduction

The picosecond excited-state lifetimes of $3d^6$ metal complexes are too short for these to be useful as practical photosensitizers.[1–5] The lifetimes for Fe(II) and Co(III) complexes can be increased with the use of strong σ-donating ligands and highly conjugated groups.[6–10] However, current ligand designs restrict the electronic density at the metal center, which limits the substrate scope for such complexes in photoredox catalysis.[2,11] Sulfur-bridged ligands with tunable oxidation states allow modulation of the electronic density at the metal center.[12] The oxidation state of the sulfur atom controls the electronic density without alteration of the metal complex core structure.

Efforts to extend the lifetime of Fe(II) complexes have focused on destabilizing the metal centered (MC) states (Fig. 1A). The fast deactivation path is restricted when MC states are higher in energy then the photoactive states, resulting in long decay lifetimes.[13–15] N-Heterocyclic carbene (NHC) and cyclometalated ligands increase the ligand field strength, but these complexes have yet to be widely used in photocatalysis.[15–17] Co(III) photosensitizers have been explored because the higher oxidation state increases the energy of the deactivating d–d states.[18–21] Most of these complexes have an extended π ligand system that lowers the energy of the lowest unoccupied molecular orbital (LUMO). The lower LUMO energy allows the photoactive state to be populated using visible light.[22–24]

Ligands containing organic chromophores enhance the photoactivity of many coordination complex-based photosensitizers.[25–29] They can extend the π conjugation in the ligands on first-row metal complexes, thereby shifting the photoactive band to lower energies.[25,28–32] Conjugated chromophores such as pyrene have also served as long-lived triplet reservoirs or as the lowest-lying excited state in metal complexes with an extended lifetime.[26,27,29] Wenger and coworkers used a carbazole group to obtain a photoactive Co(III) complex that shows a nanosecond lifetime that is active towards photoinduced electron transfer (PET) (Fig. 1B).[33] These complexes embody interesting properties, however efforts to systematically modify the electronic density at the metal center remain limited.

Our group has previously investigated how sulfur-bridged ligands can alter the photophysical properties of metal com-

[a]*Department of Chemistry, University of British Columbia, Vancouver, British Columbia V6T 1Z1, Canada. E-mail: mwolf@chem.ubc.ca*
[b]*Department of Chemistry, Simon Fraser University, Burnaby, British Columbia, V5A 1S6, Canada*

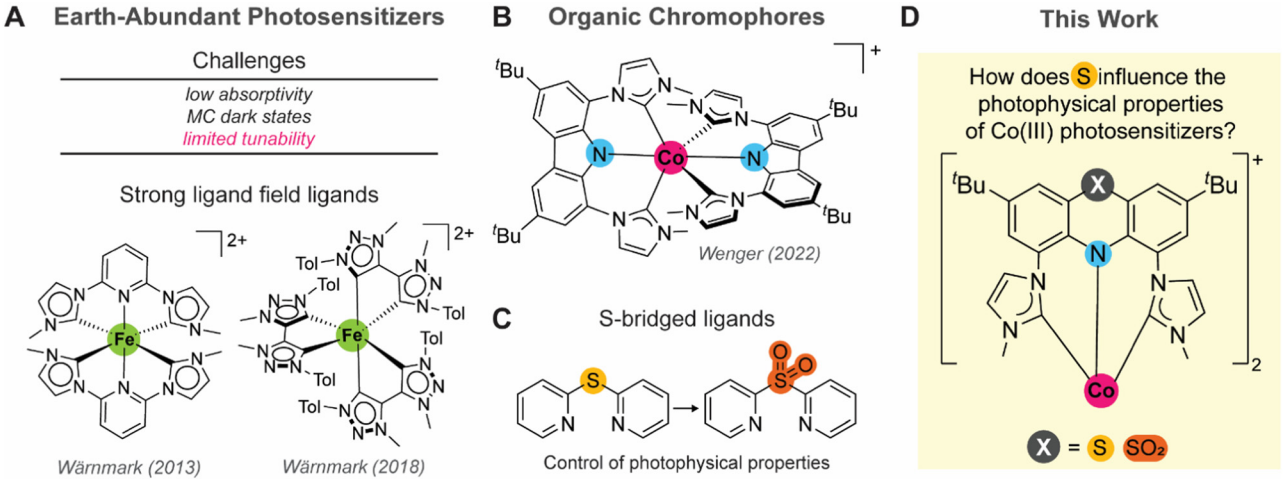

Fig. 1 (A) Challenges and ligand design proposed previously for first-row d^6 photosensitizers.[13,14] (B) Co(III) complex containing carbazole-based ligands with MLCT excited state with nanosecond lifetime.[33] (C) Sulfur-bridged ligands tune the photophysical properties of metal complexes.[12] (D) New Co(III) complexes containing phenothiazine-based ligands investigated herein.

plexes, including those based on Cu(I), Re(I), Pt(II), and Ir (III).[12,34–38] Oxidation of the sulfur bridge alters the energy of the ligand-centered molecular orbitals, thereby modulating the luminescence and ^{3}MLCT state lifetimes (Fig. 1C). Photoreduction of carbon dioxide by bimetallic rhenium(I)–ruthenium(II) dyads is also influenced by the sulfur oxidation state of a bridging ligand.[38] Recently, luminescent B(III) complexes containing a sulfur-bridge-containing amido π-donor ligand, phenothiazine, were reported. Further oxidation of sulfur in the phenothiazine altered the photophysical and electrochemical properties of the complexes.[39]

We now demonstrate use of sulfur-bridged ligands in Co(III) photosensitizers (Fig. 1D). In this work, we disclose a tridentate chelating ligand combining two σ-donating NHC units and a central phenothiazine π-donor. The sulfur bridge creates a more flexible backbone compared to other pincer-type ligands, favoring the formation of the *facial* isomer and affecting the excited-state lifetime.[33,40] The electron density at the metal center is modulated by the oxidation state of sulfur, thus dictating the excited-state dynamics. Our study also includes iron(III) analogs to better understand the impact of the sulfur-bridge ligand in their structural and electrochemical properties.

Results and discussion

Synthesis and characterization

Cobalt(III) complexes containing phenothiazine $[Co(PTZIm_2)_2]PF_6$ (**CoS**) and phenothiazine-5-5′-oxide $[Co(PTZO_2Im_2)_2]PF_6$ (**$CoSO_2$**) NHC ligands along with iron(III) analogs $[Fe(PTZIm)_2]PF_6$ (**FeS**) and $[Fe(PTZO_2Im_2)_2]PF_6$ (**$FeSO_2$**), were synthesized. The sulfur-bridged imidazolium ligands **$PTZIm_2H$** and **$PTZO_2Im_2H$** were prepared using previously published procedures with modifications (Scheme S1).[33,41] The reaction between 2.0 eq. of the corresponding ligands and 6.6 eq. of lithium bis(trimethylsilyl)amide (LiHMDS) with 1.0 eq. of the cobalt(II) bromide or iron(II) bromide in THF at −78 °C led to the corresponding cobalt(III) and iron(III) complexes after exposure to air, with yields between 29% and 44% (Fig. 2A).

The diamagnetic Co(III) complexes were characterized by ^{1}H, $^{13}C\{^1H\}$, $^{31}P\{^1H\}$ and $^{19}F\{^1H\}$ NMR spectroscopies, X-ray crystallography, HR-ESI mass spectrometry and infrared spectroscopy (FT-IR). The paramagnetic Fe(III) complexes were characterized by FT-IR, HR-ESI mass spectrometry, EPR spectroscopy, and X-ray crystallography. Symmetric stretching of the sulfone (SO_2) at 1135 and 1129 cm^{-1} in the FT-IR spectra, is observed in **$CoSO_2$** and **$FeSO_2$** respectively, but is absent in **CoS** and **FeS**. Additionally, a stretching peak at 833 cm^{-1} confirms that PF_6^- is the counterion for all complexes (Fig. S1 and S2). HR-ESI mass spectra show peaks corresponding to the molecular ions with characteristic cobalt and iron isotopic patterns (Fig. S6–S9). The protons characteristic of the imidazolium groups in **$PTZIm_2H$** and **$PTZO_2Im_2H$**, at 8.53 ppm and 8.69 ppm in the ^{1}H NMR spectra, respectively, are absent in the spectra of **CoS** and **$CoSO_2$** (Fig. S12–S23). Two sets of ligand peaks in the ^{1}H and $^{13}C\{^1H\}$ NMR spectra of the complexes indicate that they adopt a *facial* arrangement. New peaks in the $^{13}C\{^1H\}$ NMR spectra between 174.5 and 160.3 ppm are characteristic of the ligating carbon atom of the NHC units. These results are in line with observations in previously reported Co(III)-NHC complexes.[20,29,33] In addition, $^{31}P\{^1H\}$ and $^{19}F\{^1H\}$ NMR spectra show the expected PF_6 signal between −143.1 and −142.7 ppm and between −73.5 and −70.3 ppm, respectively, with J_{P-F} = 700 Hz.

X-band EPR spectra of the iron(III) complexes in acetonitrile at 298 K show broad signals consistent with low-spin d^5 Fe(III) centers.[15,31,33,42] These spectra were simulated as isotropic signals with g = 2.0752 for **FeS** (Fig. S24) and g = 2.1410 for

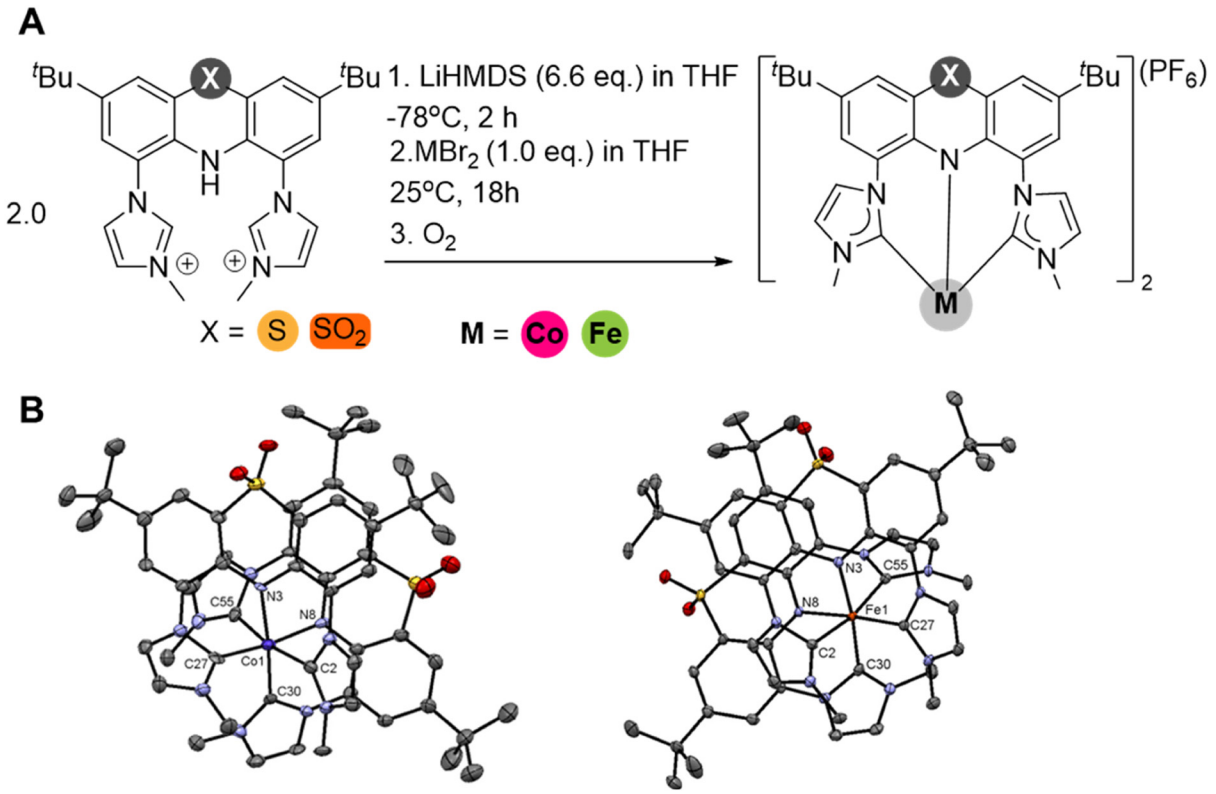

Fig. 2 (A) Synthesis route using LiHMDS as a base and subsequent metalation with corresponding metal bromide salt to obtain Co(III) and Fe(III) complexes. (B) Perspective drawing of $\mathbf{CoSO_2}$ (left) and $\mathbf{FeSO_2}$ (right). Ellipsoids are plotted at the 50% probability level. Solvent molecules and H atoms are removed for clarity.

$\mathbf{FeSO_2}$ (Fig. S25). The higher *g* value for $\mathbf{FeSO_2}$ is assigned to the greater electron-withdrawing effect of the SO_2 group, which increases delocalization of unpaired electron density onto the ligand, impacting both the ligand field splitting and bond covalency.[31,43,44] Similar effects have been reported from electron withdrawing groups in other amido-bridged metal complexes.[44] Small signals (<1%) are tentatively attributed to minor amounts of an additional Fe(III) complex and uncomplexed phenothiazine radicals.[45,46]

Single crystal X-ray diffraction (XRD) analysis confirmed that $\mathbf{CoSO_2}$ and $\mathbf{FeSO_2}$ crystallized in the *facial* geometry (Fig. 2B and Tables S1–S3). Both complexes adopt a distorted octahedral geometry with N_{amido}–M–C_{NHC} axial angles in the range of 172.7(2) to 175.5(2)° for $\mathbf{CoSO_2}$ and 173.26(10) and 175.65(11)° for $\mathbf{FeSO_2}$. The Co–N_{amido} bond length is 2.045(5) Å in $\mathbf{CoSO_2}$ and the Fe–N_{amido} bond length in $\mathbf{FeSO_2}$ is 2.026(2) Å. These values are longer than in some other amido-bridged complexes, resulting from the electron withdrawing ability of the SO_2 group, which weakens the amido bond and reduces the covalent character.[31,33,47] The Co–C_{NHC} bond length *trans* to the amido groups averages 1.938(2) Å in $\mathbf{CoSO_2}$ and 1.984(8) Å in $\mathbf{FeSO_2}$. These are shorter than the axial Co–C_{NHC} bonds in $\mathbf{CoSO_2}$ (1.994(6) Å) and $\mathbf{FeSO_2}$ (2.025(3) Å), attributed to the SO_2 group. The overall values are in line with other iron(III) and cobalt(III) NHC complexes.[17,29,31,32] Helical twisting in the coordination environment is associated with *P*- and *M*-chirality.[48] In both cases, the packing structure indicates the co-crystallization of two different enantiomers as a *P*- and *M*-pair (Fig. S26). Similar complexes containing Co(III), Fe(III) and Cr(III) also show the same behavior.[32,33,49,50] Intramolecular phenothiazine-5-5′-oxide ring distances between 3.492 and 3.506 Å in both complexes indicate π···π stacking interactions in the solid state.

Structural analysis of the ground state geometry of $\mathbf{CoSO_2}$ using B3LYP/DEF2-tzvp(-f) with ZORA scalar relativistic corrections is in good agreement with the crystal structure (Table S5). The average error in the bond length is 1.06%, and 1.59% for coordinating bond angles. We also modelled the structure of **CoS** using DFT, which shows a shorter Co–N_{amido} bond length of 2.0110 Å, comparable to other amido-bridged complexes.[31,33] Complex **CoS** exhibits a larger distortion from a perfect octahedral geometry, with an average N_{amido}–Co–C_{NHC} axial angle of 168.47°. The lowest-lying triplet geometry (T_1) of both complexes was optimized with the unrestricted DFT method (Table S6). Overall, the Co–N_{amido} and *trans* C–C_{NHC} bond lengths increase, and the axial Co–C_{NHC} bonds shorten relative to the ground state. The complexes show root-mean-square deviations (RMSDs) of 0.333 for **CoS** and 0.314 for $\mathbf{CoSO_2}$ between the ground state and T_1 geometries, in line with the greater distortion expected in **CoS**.

Ground-state spectroscopy

We investigated the electronic properties of the Co(III) complexes and ligands in acetonitrile solutions using UV-vis spectroscopy (Fig. 3A, Fig. S27 and Table 1). The absorption spectra of **CoS** and **$CoSO_2$** show bands between 350 and 450 nm, distinct from the free ligands. **CoS** displays a broad band peaking at 392 nm, assigned as a mixture of metal/ligand-to-ligand charge-transfer ((M + L)LCT) [d(Co) + $\pi(N_{amido}) \rightarrow \pi^*(C_{NHC})$] and metal-centered (MC) [d(Co) → d*(Co)] transitions according to the computational studies discussed below. The **$CoSO_2$** complex shows a band at 402 nm, assigned to a mixture of (M + L)LCT [d(Co) + $\pi(N_{amido}) \rightarrow \sigma^*(C_{NHC})$] and MC [d(Co) → d*(Co)] states (Fig. 3D). The Co(III) complexes reported here show similar features as seen in other Co(III) NHC complexes.[20,33] Complexes of the SO_2 series show a distinct band with high absorptivity (~10^4 L mol^{-1} cm^{-1}) peaking at 336 nm in **$CoSO_2$** and 331 nm in **$FeSO_2$** assigned to predominantly intraligand charge transfer (ILCT) between phenothiazine-5-5′-oxide ligands and minor MC character (Fig. S34, state S_{14}). Ligand **$PTZO_2Im_2H$** shows a similar feature at 339 nm, in line with the band assignment as predominantly ligand-based. Complex **FeS** shows a band at 800 nm and **$FeSO_2$** bands at 789 nm and 903 nm, similar to other iron(III) and iron(II) complexes containing amido bridge ligands (Fig. 3B).[31,33,51,52] The "HOMO inversion" lowers the bandgap by mixing 3d metal orbitals with $\pi(N_{amido})$ orbitals. We also observed an increase in the absorptivity in iron(III), with $\varepsilon = 10^3$ L mol^{-1} cm^{-1}, higher than for a typical d–d transition. The oxidation of sulfur causes a blue-shifted absorption in **$FeSO_2$** compared to **FeS** caused by the electron withdrawing ability of SO_2 which lowers the 3d orbital energies.

Time-dependent density functional theory (TD-DFT) simulated spectra show good agreement with experimental data

Table 1 Electronic absorption data of complexes **CoS**, **$CoSO_2$**, **FeS** and **$FeSO_2$** and ligands **$PTZIm_2H$** and **$PTZO_2Im_2H$** in acetonitrile solution (2 × 10^{-5} mol L^{-1})

Entry	Compound	Absorption/λ_{abs} [nm] (ε/L mol^{-1} cm^{-1})
1	**$PTZIm_2H$**	258 (3500), 327 (500)
2	**$PTZO_2Im_2H$**	276 (13 000), 339 (6800), 358 (5500), 409 (400), 424 (400)
3	**CoS**	260 (38 600), 392 (10 000), 488[a] (1000)
4	**$CoSO_2$**	336 (16 900), 402 (10 000), 455[a] (800)
5	**FeS**	267 (27 300), 379 (8900), 414[a] (6800), 800 (2000)
6	**$FeSO_2$**	331 (21 200), 719 (2600), 903 (2300)

[a] Shoulder.

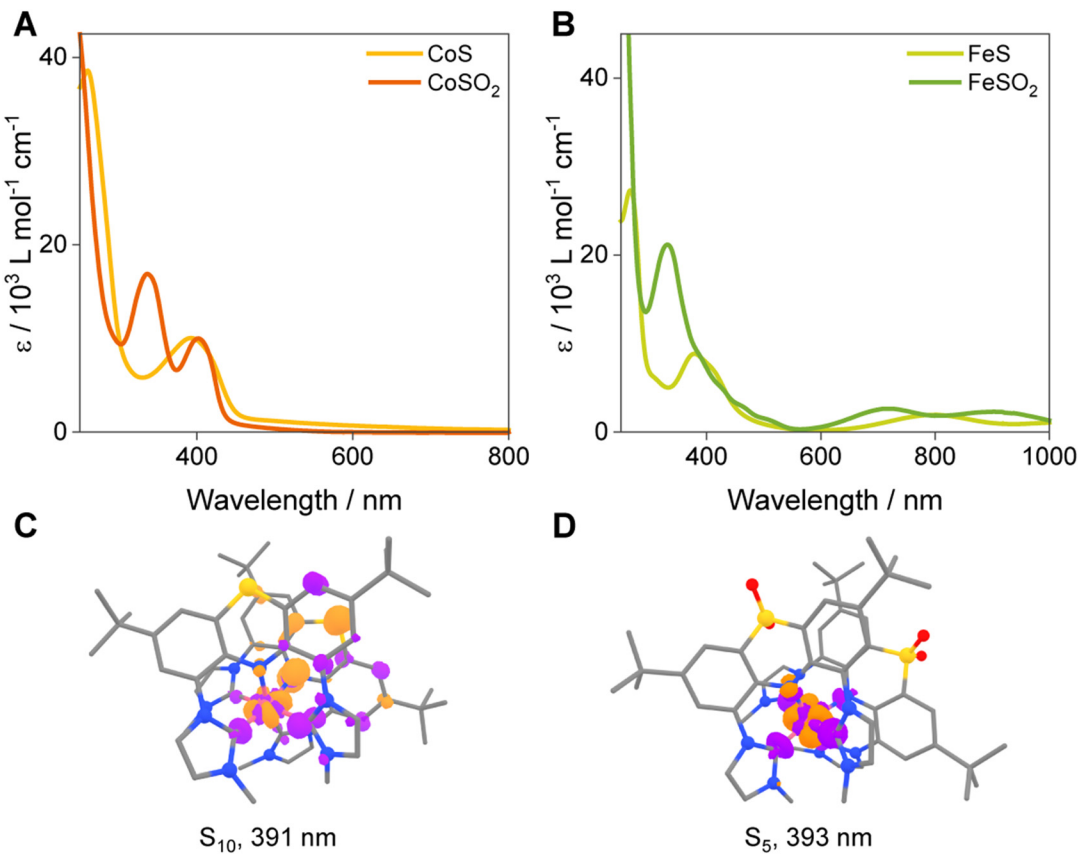

Fig. 3 UV-vis absorption spectra of **CoS** and **$CoSO_2$** (A), and **FeS** and **$FeSO_2$** (B) in acetonitrile at 298 K. Electron density difference plot for S_{10} at 391 nm of **CoS** (C) and S_5 at 393 nm of **$CoSO_2$** (D), based on TD-DFT calculations. The orange region shows depletion, and the purple region shows a gain in electron density.

(Fig. S29–S35 and Tables S7–S8). For **CoS**, an electron density difference map of state S_{10} at 391 nm shows a (M + L)LCT transition with electron density depletion (orange) localized on the metal center, amido nitrogen and sulfur atoms, and density gain (purple) at the metal center and NHC ligands (Fig. 3C). This state is composed of a mixture of 20% HOMO → LUMO+4, 11% HOMO → LUMO+3 and 11% HOMO−1 → LUMO+3 transitions. Similar character and oscillator strength is found in the S_{11} state at 391 nm and S_{14} at 329 nm. The density map of state S_5 **$CoSO_2$** at 393 nm shows electron depletion at both the metal center and the amido nitrogen, with increased density at the cobalt d-orbitals and the phenothiazine moiety (Fig. 3D). This state has mixed (M + L)LCT/MC character and is composed of 46% HOMO → LUMO+1 and 44% HOMO → LUMO transitions. The oxidation also causes a blue shift of the absorption to the S_1 state from 575 nm in **CoS** to 482 nm in **$CoSO_2$** where both transitions have low oscillator strength (>0.0005). The oxidation of the sulfur atom lowers the energy of the ligand orbitals, caused by the electron-withdrawing ability of the SO_2 moiety compared to sulfide. This is in line with the cyclic voltammetry data shown below. Higher-energy transitions show π → π*, MLCT and LLCT character with low oscillator strengths.

Electrochemistry and spectroelectrochemistry

The redox behaviour of the complexes in 0.1 M (^{n}Bu$_4$N)PF$_6$ acetonitrile solution was examined with cyclic voltammetry (CV). Redox assignments from the cyclic voltammograms in Fig. 4A are shown in Table 2, based on the spectroelectrochemistry data shown below and comparison with similar compounds and ligands (Fig. S36).[33,39] **$CoSO_2$** exhibits a chemically irreversible wave at E_{pc} = −1.54 V *vs.* $Fc^{+/0}$ assigned as ligand reduction. No reduction event associated with the $Co^{III/II}$ couple is observed. This is attributed to the strongly electron-donating nature of the ligand and the complexes possess similar values to other NHC-based Co(III) complexes.[20,29,33] **FeS** and **$FeSO_2$** display two chemically reversible reduction waves at $E_{1/2}$ = −1.40 and −0.78 V *vs.* $Fc^{+/0}$, respectively, assigned to the $Fe^{III/II}$ reduction couples. The reduction potential is positively shifted in the SO_2 complexes as the amido σ donation is weakened with greater oxidation of sulfur, stabilizing the d*(Fe) orbitals. Similarly, the $Fe^{IV/III}$ oxidation couple is anodically shifted in **$FeSO_2$** relative to in **FeS**, resulting from the influence of HOMO inversion on the d orbital energies. This effect is greater than in other Fe(III) complexes containing electron withdrawing/donating groups.[25,53,54]

Three chemically reversible oxidation waves are observed in **CoS** and **FeS** (Table 2, entries 1 and 5). The first wave at −0.32 V *vs.* $Fc^{+/0}$ for **CoS** and −0.35 V *vs.* $Fc^{+/0}$ for **FeS** is absent in the SO_2 complexes and in the carbazole series and is assigned to one-electron oxidation of the phenothiazine.[39] The second wave is cathodically shifted from +0.21 in **FeS** to +0.02 V *vs.* $Fc^{+/0}$ in **CoS**. These are assigned to the $Fe^{IV/III}$ and $Co^{IV/III}$

Table 2 Electrochemical potentials (in V *vs.* $Fc^{+/0}$) of **CoS**, **$CoSO_2$**, **FeS** and **$FeSO_2$** and previously reported NHC complexes of cobalt(III) and iron(III)

Entry	Compound	$E_{1/2red}$[a]	$E_{1/2}$[a] ($L^{\bullet+/0}$)	$E_{1/2}$[a] ($M^{IV/III}$)	$E_{1/2}$[a] ($L^{2+/\bullet+}$)
1	**CoS**	N/A	−0.32	+0.02	+0.83
2	**$CoSO_2$**	−1.54[b]	+0.51	+0.77[b]	N/A
3	$[Co(L^{CNC})_2]^{+}$ [c]	−2.21[b]	+0.72	+0.42	N/A
4	$[Co(PhB(MeIm)_3)_2]^{+}$ [d]	N/A	+1.55	+0.96	+1.76
5	**FeS**	−1.40	−0.35	+0.21	+0.78
6	**$FeSO_2$**	−0.78	+0.44	+0.95[b]	N/A
7	$[Fe(L^{CNC})_2]^{+}$ [c]	−1.38	+0.56	+0.05	N/A

[a] Potential referenced to $Fc^{+/0}$ in V. [b] Irreversible wave. [c] L^{CNC} = 3,3′-(3,6-di-*tert*-butylcarbazole-9-id-1,8-diyl)bis(1-methyl-1*H*-imidazol-3-ium-2-ide) (Fig. 1B).[33] [d] PhB(MeIm)$_3$ = tris(3-methylimidazolin-2ylidene)(phenyl)borate.[20]

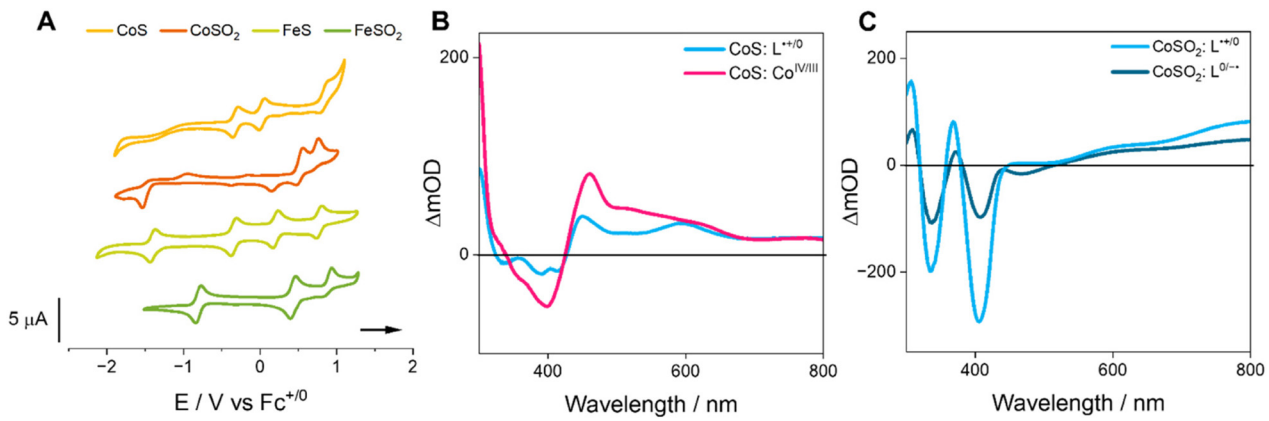

Fig. 4 (A) Cyclic voltammograms in argon-sparged dry acetonitrile in 0.1 M (^{n}Bu$_4$N)(PF$_6$) at 298 K of **CoS**, **$CoSO_2$**, **FeS** and **$FeSO_2$** (1 mM) swept anodically at a scan rate of 100 mV s^{-1}, and initiated at the open circuit potential (**CoS**: −0.6 V *vs.* $Fc^{+/0}$; **$CoSO_2$**: −0.5 V *vs.* $Fc^{+/0}$; **FeS**: −1.0 V *vs.* $Fc^{+/0}$; **$FeSO_2$**: −0.6 V *vs.* $Fc^{+/0}$). (B) UV-vis changes following ligand-based oxidation (light blue, scanning from −0.60 to −0.02 V *vs.* $Fc^{+/0}$) and metal-based oxidation (pink, scanning from −0.02 to +0.40 V *vs.* $Fc^{+/0}$) of **CoS** in de-aerated acetonitrile at 298 K. (C) UV-vis changes following ligand-based oxidation (light blue, scanning from 0 to −0.70 V *vs.* $Fc^{+/0}$) and ligand-based reduction (dark blue, scanning from 0 to −1.80 V *vs.* $Fc^{+/0}$) of **$CoSO_2$** in de-aerated acetonitrile at 298 K.

couples, respectively. The combination of σ- and π-donor properties with the addition of sulfur results in a higher donating ability of **CoS** in comparison with the carbazole-based Co(III) complex (Table 2, entry 3), lowering the oxidation potential of the $Co^{IV/III}$ oxidation couple.[33,39] The third wave shows similar values of +0.83 V *vs.* $Fc^{+/0}$ in **CoS** and +0.78 V *vs.* $Fc^{+/0}$ in **FeS**, assigned to the second oxidation of the phenothiazine unit.[39]

Complex **$CoSO_2$** shows two chemically irreversible oxidation processes at +0.51 and +0.77 V *vs.* $Fc^{+/0}$, assigned to ligand and $Co^{IV/III}$ oxidation, respectively (Table 2, entry 2). The reversibility of the ligand oxidation is influenced by the metal oxidation event (Fig. S37). When scanned past +0.77 V *vs.* $Fc^{+/0}$, the event at +0.51 V *vs.* $Fc^{+/0}$ is chemically irreversible. However, this wave becomes more reversible when the potential is limited to +0.65 V *vs.* $Fc^{+/0}$. We also observed the disappearance of the wave at +0.15 V *vs.* $Fc^{+/0}$, suggesting that a chemical step takes place upon oxidation of Co^{III} to Co^{IV} at +0.77 V *vs.* $Fc^{+/0}$. A cathodic shift greater than 0.73 V is observed in the $M^{IV/III}$ oxidation couple between the S and SO_2 series. This result showcases the influence of the oxidation state of the sulfur on the electronic density of the metal, which is greater than in other S-bridged metal complexes.[34–38]

Spectroelectrochemistry experiments support the CV assignments and help rationalize the character of the excited states (Fig. 4B, C and Fig. S38–S46). Upon oxidation of the ligand at −0.35 V *vs.* $Fc^{+/0}$, **CoS** shows a decrease in the intensity of the bands at 332, 388 and 413 nm and an increase in the bands at 450 and 596 nm. These spectral changes are attributed to a single-electron transfer to generate a phenothiazine radical, consistent with observations in other phenothiazine-based complexes.[55,56] **FeS** shows an increase in the band at 596 nm in the same voltage range, supporting the phenothiazine oxidation assignment (Fig. S42). When the potential is scanned past +0.40 V *vs.* $Fc^{+/0}$, the band at 392 nm decreases in intensity while the band at 460 nm increases, supporting assignment of the wave as $Co^{IV/III}$. These results are consistent with the (M + L)LCT nature of the 392 nm band as predicted by TD-DFT. **$CoSO_2$** shows similar features when scanned to +0.7 V *vs.* $Fc^{+/0}$ and −1.8 V *vs.* $Fc^{+/0}$, supporting the ligand character of the redox events. In both cases, the bands at 335 and 406 nm show depletion and bands at 307, 368, 800 nm increase in intensity. The observed spectral changes align with ligand events observed in spectroelectrochemistry of **$FeSO_2$**. Upon oxidation of the ligand at +0.44 V *vs.* $Fc^{+/0}$, the band at 331 nm decreases in intensity and a broad band spanning from 600 to 900 nm increases in intensity (Fig. S45).

Excited-state dynamics

We used femtosecond transient absorption (fsTA) to investigate the non-radiative decay lifetimes of the complexes **CoS** and **$CoSO_2$**. Upon excitation at 400 nm, **CoS** shows a ground-state bleach (GSB) at 392 nm and excited-state absorption (ESA) bands at 448 nm and 565 nm (Fig. S47–S48). Global analysis of the transient absorption data yielded four exponential decays: lifetimes of 0.2 ps, 3.3 ps, 35.1 ps and 8.0 ns (Fig. 5A). The 0.2 ps component shows broad spectral features between

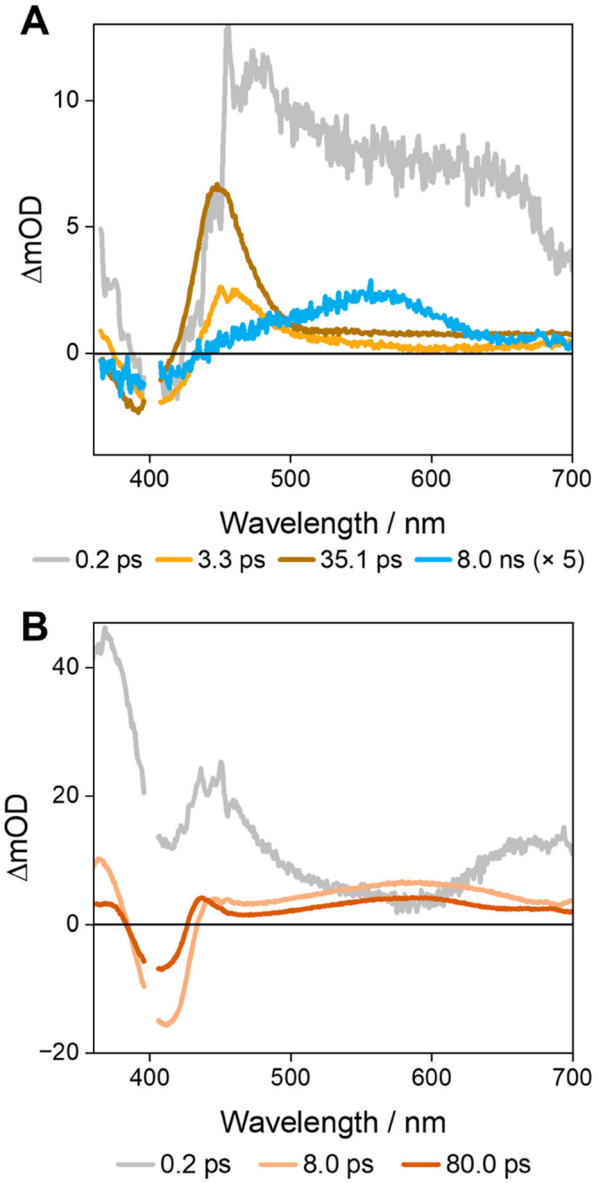

Fig. 5 Decay-associated spectra (DAS) of **CoS** (A) and **$CoSO_2$** (B) obtained from femtosecond transient absorption in de-aerated acetonitrile at 298 K prompted by a 400 nm excitation source.

440 and 700 nm and between 350 and 380 nm. We propose that this component is associated with vibrational cooling and an intersystem crossing that the ^{1}(M + L)LCT state undergoes, similar to other d^6 metal complexes.[57–61] The 3.3 ps and 35.1 ps components are associated with the 392 and 448 nm bands. Both components are associated with ^{3}MC states as suggested by spectroelectrochemical results and SOC-TD-DFT (Table S9 and Fig. S33).[62] The long-lived 8.0 ns component exhibits bands at 392 and 565 nm. The 565 nm band corresponds to a one-electron oxidized phenothiazine radical unit, as observed in the spectroelectrochemistry experiments discussed above and other compounds containing phenothiazine.[63–65] We thus tentatively assign the long component as having primarily triplet phenothiazine character, as

also predicted by the SOC-TD-DFT results (Fig. S33 and Table S9).

Complex **$CoSO_2$** shows a GSB at 402 nm and ESAs at 350 nm, 436 and 590 nm (Fig. S49 and S50). Four decay-associated spectra (DAS) are associated with the excited-state dynamics: 0.002, 0.2, 8.0 and 80.0 ps (Fig. 5B). The shortest component (0.002 ps) accounts for the coherent and solvent effects and is excluded from the excited-state dynamics.[57,66] The 0.2 ps component shows ESAs at 368, 450 and 693 nm. This component is also tentatively assigned to vibrational relaxation of the singlet excited state followed by intersystem crossing (ISC) to the lowest triplet vibrational state.[57–61] The 8.0 ps component is associated with signals at 363, 411, and 590 nm, while the longer 80.0 ps component correspond to bands at 371, 408, 437 and 590 nm. These features do not fully match with the spectroelectrochemical spectra following ligand oxidation and reduction, particularly the band at 436 nm. We hypothesize that these decay components are associated with ^{3}MC states based on the SOC-TD-DFT results (Table S9 and Fig. S34). Their lifetimes are longer than the fast decay components observed in **CoS**. Both energetic and structural effects could be playing a role in the extension of the decay lifetimes. The energy of the T_1 state in **$CoSO_2$** is 0.3 eV higher than in **CoS**. We expected that the lower T_1 energy would increase the non-radiative rate constant, decreasing the decay lifetime.[67] Oxidation of the sulfur atom could also increase ligand rigidity, thereby extending the ^{3}MC state lifetimes. This is evidenced by the larger RMSD between the T_1 and S_0 states in **CoS** compared to **$CoSO_2$** in the optimized DFT structures (Table S6), suggesting that the T_1 state is more distorted in **CoS**, facilitating non-radiative decay. The same effect is observed in B(III) complexes containing phenothiazine and other sulfur-bridged complexes reported in our group, where non-radiative decay is slower upon sulfur oxidation.[12,34–39]

The ^{2}LMCT state is populated in complexes **FeS** and **$FeSO_2$** when excited at 400 nm. The fsTA spectra of **FeS** display an increase in intensity at 460 and 550 nm and a depletion at 380 and 700 nm. **$FeSO_2$** shows ESAs at 368 and 585 nm, and a small GSB at 700 nm (Fig. S51–S55). Global analysis of **FeS** yielded three components that are associated with the internal conversion (0.2 ps), ^{2}LMCT decay (0.8 ps) and ^{3}MC (11.5 ps) (Fig. S53). We observed an increase in the decay lifetime upon oxidation of the sulfur, similarly to in the cobalt(III) complexes. In the case of **$FeSO_2$** the global analysis showed components of 0.3 ps associated with internal conversion and 8.3 ps associated with ^{2}LMCT decay. A long component with a lifetime of 741.9 ps could originate from a high-spin iron(III) complex, as has also been observed in another amido-bridged iron(II) complex (Fig. S54–S56).[68] Both complexes show decay lifetimes comparable to the Fe(III) carbazole-NHC complex and are two to three orders of magnitude shorter than in other recently reported Fe(III) complexes.[17,33,42,69,70]

We observed a substantial increase in the lifetime when comparing the Fe(III) and Co(III) complexes. The higher nuclear charge in Co(III) could increase the energy of the MC states, leading to longer lifetimes. On the other hand, the d^5 Fe(III) complexes show sub-picosecond lifetimes. "HOMO inversion" achieved with the amido-bridged ligand lowers the energy of the charge transfer band to extend the decay lifetime in Fe(II) complexes. This is not beneficial for the Fe(III) series, as it requires strong ligand field ligands to achieve longer lifetimes.[14,17,42,70] In the Fe d^5 system, organic chromophores are effective in extending lifetimes when not directly bonded to the metal center.[25,28]

Finally, we examined whether radiative decay could occur in any of the complexes or ligands. **$PTZIm_2H$** and **$PTZO_2Im_2H$** show a broad blue/green emission in acetonitrile with maxima at 432 and 493 nm, respectively (Fig. S28). Both display decay lifetimes in the nanosecond range with quantum yields (Φ_{em}) of 0.9% for **$PTZIm_2H$** and 1.3% **$PTZO_2Im_2H$** (Table S4). These results are similar to other ligands containing phenothiazine units.[39] Photoluminescence was not observed in complexes at 298 and 77 K under inert conditions. These results suggest that non-radiative decay is the major decay path in these complexes.

Conclusions

This study presents a method to control the electronic density in Co(III) photosensitizers using sulfur-bridged ligands. Changing the oxidation state of sulfur in the Co(III) complexes led to three key insights. First, the more flexible backbone of the ligands relative to other pincer-type ligands favoured the formation of *facial* isomers. NMR spectroscopies and XRD confirmed the presence of the *facial* isomer in solid and in solution. This structural flexibility likely contributes to the observed fast decay components and alters the excited state character of the complexes. Second, the oxidation state of sulfur modulated the metal electronic density. Cyclic voltammetry experiments showed that the higher donating nature of the **$PTZIm_2H$** ligand favours the formation of $M^{IV/III}$ for both **CoS** and **FeS**. Oxidation to SO_2 cathodically shifted the oxidation couples. This effect is greater than for other sulfur-bridged ligands previously reported in our group.[35–37] UV-vis spectra and TD-DFT analysis also revealed that the phenothiazine unit has less contribution to the band at 400 nm after sulfur oxidation in **$CoSO_2$**. Finally, excited state dynamics depended on the oxidation state of sulfur. Transient absorption experiments showed that the phenothiazine in **CoS** facilitated fast non-radiative channels, however a long component >8.0 ns is observed. Oxidation of the S in **$CoSO_2$** reduced the non-radiative rate and increased the lifetime of the short components. These results show that sulfur oxidation state can be used to control the photophysics of first-row photosensitizers beyond traditional ligand designs.

Author contributions

J. T., K. M. T. and M. O. W. wrote the manuscript. J. T. carried out the synthesis, characterization, photophysical properties

and DFT calculations. K.-M. T. and B. O. P. collected and refined the XRD structures. S. K. carried out time-resolved measurements and global analysis of the spectroscopic data. C. J. W. collected and simulated the EPR data. M. O. W. supervised the project. All authors discussed the progress of the research and reviewed the manuscript.

Conflicts of interest

The authors declare no competing financial interest.

Data availability

The data supporting this study can be found in the article or in the supplementary information (SI). Supplementary information: all experimental procedures, FT-IR, EPR and NMR spectra, HR-ESI mass spectra, crystal and structure determination data, additional photophysical, electrochemical and computational data. See DOI: **https://doi.org/10.1039/d5qi02362a**.

CCDC 2480167 and 2480168 contain the supplementary crystallographic data for this paper.[71a,b]

Acknowledgements

This work was supported by the Natural Sciences and Engineering Research Council of Canada (NSERC). We would like to acknowledge the Laboratory for Advanced Spectroscopy and Imaging Research (LASIR) for facility access.

References

1 J.-H. Shon and T. S. Teets, Photocatalysis with Transition Metal Based Photosensitizers, *Comments Inorg. Chem.*, 2020, **40**, 53–85.
2 A. Y. Chan, I. B. Perry, N. B. Bissonnette, B. F. Buksh, G. A. Edwards, L. I. Frye, O. L. Garry, M. N. Lavagnino, B. X. Li, Y. Liang, E. Mao, A. Millet, J. V. Oakley, N. L. Reed, H. A. Sakai, C. P. Seath and D. W. C. MacMillan, The Merger of Photoredox and Transition Metal Catalysis, *Chem. Rev.*, 2022, **122**, 1485–1542.
3 J. K. McCusker, Electronic Structure in the Transition Metal Block and Its Implications for Light Harvesting, *Science*, 2019, **363**, 484–488.
4 G. Morselli, C. Reber and O. S. Wenger, Molecular Design Principles for Photoactive Transition Metal Complexes: A Guide for "Photo-Motivated" Chemists, *J. Am. Chem. Soc.*, 2025, **147**, 11608–11624.
5 C. Förster and K. Heinze, Photophysics and Photochemistry with Earth-Abundant Metals – Fundamentals and Concepts, *Chem. Soc. Rev.*, 2020, **49**, 1057–1070.
6 O. S. Wenger, A Bright Future for Photosensitizers, *Nat. Chem.*, 2020, **12**, 323–324.
7 B. M. Hockin, C. Li, N. Robertson and E. Zysman-Colman, Photoredox Catalysts Based on Earth-Abundant Metal Complexes, *Catal. Sci. Technol.*, 2019, **9**, 889–915.
8 D. Kim, V. Q. Dang and T. S. Teets, Improved Transition Metal Photosensitizers to Drive Advances in Photocatalysis, *Chem. Sci.*, 2024, **15**, 77–94.
9 D. M. Arias-Rotondo and J. K. McCusker, The Photophysics of Photoredox Catalysis: A Roadmap for Catalyst Design, *Chem. Soc. Rev.*, 2016, **45**, 5803–5820.
10 N. Sinha and O. S. Wenger, Photoactive Metal-to-Ligand Charge Transfer Excited States in $3d^6$ Complexes with Cr^0, Mn^I, Fe^{II}, and Co^{III}, *J. Am. Chem. Soc.*, 2023, **145**, 4903–4920.
11 T. Huang, P. Du and Y.-M. Lin, Recent Advances in Photoactive First-Row Transition Metal Complexes for Organic Synthesis, *Chin. J. Chem.*, 2025, **43**, 2566–2587.
12 J. Yuan, Z. Xu and M. O. Wolf, Sulfur-Bridged Chromophores for Photofunctional Materials: Using Sulfur Oxidation State to Tune Electronic and Structural Properties, *Chem. Sci.*, 2022, **13**, 5447–5464.
13 Y. Liu, T. Harlang, S. E. Canton, P. Chábera, K. Suárez-Alcántara, A. Fleckhaus, D. A. Vithanage, E. Göransson, A. Corani, R. Lomoth, V. Sundström and K. Wärnmark, Towards Longer-Lived Metal-to-Ligand Charge Transfer States of Iron(II) Complexes: An N-Heterocyclic Carbene Approach, *Chem. Commun.*, 2013, **49**, 6412–6414.
14 P. Chábera, K. S. Kjaer, O. Prakash, A. Honarfar, Y. Liu, L. A. Fredin, T. C. B. Harlang, S. Lidin, J. Uhlig, V. Sundström, R. Lomoth, P. Persson and K. Wärnmark, Fe^{II} Hexa N-Heterocyclic Carbene Complex with a 528 ps Metal-to-Ligand Charge-Transfer Excited-State Lifetime, *J. Phys. Chem. Lett.*, 2018, **9**, 459–463.
15 W. Leis, M. A. Argüello Cordero, S. Lochbrunner, H. Schubert and A. A. Berkefeld, A Photoreactive Iron(II) Complex Luminophore, *J. Am. Chem. Soc.*, 2022, **144**, 1169–1173.
16 O. S. Wenger, Is Iron the New Ruthenium?, *Chem. – Eur. J.*, 2019, **25**, 6043–6052.
17 K. S. Kjær, N. Kaul, O. Prakash, P. Chábera, N. W. Rosemann, A. Honarfar, O. Gordivska, L. A. Fredin, K.-E. Bergquist, L. Häggström, T. Ericsson, L. Lindh, A. Yartsev, S. Styring, P. Huang, J. Uhlig, J. Bendix, D. Strand, V. Sundström, P. Persson, R. Lomoth and K. Wärnmark, Luminescence and Reactivity of a Charge-Transfer Excited Iron Complex with Nanosecond Lifetime, *Science*, 2019, **363**, 249–253.
18 A. Ghosh, J. T. Yarranton and J. K. McCusker, Establishing the Origin of Marcus-Inverted-Region Behaviour in the Excited-State Dynamics of Cobalt(III) Polypyridyl Complexes, *Nat. Chem.*, 2024, **16**, 1665–1672.
19 A. Y. Chan, A. Ghosh, J. T. Yarranton, J. Twilton, J. Jin, D. M. Arias-Rotondo, H. A. Sakai, J. K. McCusker and D. W. C. MacMillan, Exploiting the Marcus Inverted Region for First-Row Transition Metal–Based Photoredox Catalysis, *Science*, 2023, **382**, 191–197.

20 S. Kaufhold, N. W. Rosemann, P. Chábera, L. Lindh, I. B. Losada, J. Uhlig, T. Pascher, D. Strand, K. Wärnmark, A. Yartsev and P. Persson, Microsecond Photoluminescence and Photoreactivity of a Metal-Centered Excited State in a Hexacarbene–Co(III) Complex, *J. Am. Chem. Soc.*, 2021, **143**, 1307–1312.

21 S. T. Burton, G. Lee, C. E. Moore, C. S. Sevov and C. Turro, Cyclometallated Co(III) Complexes with Lowest-Energy Charge Transfer Excited States Accessible with Visible Light, *J. Am. Chem. Soc.*, 2025, **147**, 13315–13327.

22 P. Zimmer, L. Burkhardt, R. Schepper, K. Zheng, D. Gosztola, A. Neuba, U. Flörke, C. Wölper, R. Schoch, W. Gawelda, S. E. Canton and M. Bauer, Towards Noble-Metal-Free Dyads: Ground and Excited State Tuning by a Cobalt Dimethylglyoxime Motif Connected to an Iron N-Heterocyclic Carbene Photosensitizer, *Eur. J. Inorg. Chem.*, 2018, **2018**, 5203–5214.

23 M. M. Alowakennu, A. Ghosh and J. K. McCusker, Direct Evidence for Excited Ligand Field State-Based Oxidative Photoredox Chemistry of a Cobalt(III) Polypyridyl Photosensitizer, *J. Am. Chem. Soc.*, 2023, **145**, 20786–20791.

24 A. K. Pal, C. Li, G. S. Hanan and E. Zysman-Colman, Blue-Emissive Cobalt(III) Complexes and Their Use in the Photocatalytic Trifluoromethylation of Polycyclic Aromatic Hydrocarbons, *Angew. Chem., Int. Ed.*, 2018, **57**, 8027–8031.

25 J. Wellauer, B. Pfund, I. Becker, F. Meyer, A. Prescimone and O. S. Wenger, Iron(III) Complexes with Luminescence Lifetimes of up to 100 ns to Enhance Upconversion and Photocatalysis, *J. Am. Chem. Soc.*, 2025, **147**, 8760–8768.

26 C. Wegeberg, D. Häussinger and O. S. Wenger, Pyrene-Decoration of a Chromium(0) Tris(Diisocyanide) Enhances Excited State Delocalization: A Strategy to Improve the Photoluminescence of 3d6 Metal Complexes, *J. Am. Chem. Soc.*, 2021, **143**, 15800–15811.

27 D. Kim, M. C. Rosko, F. N. Castellano, T. G. Gray and T. S. Teets, Long Excited-State Lifetimes in Three-Coordinate Copper(I) Complexes via Triplet–Triplet Energy Transfer to Pyrene-Decorated Isocyanides, *J. Am. Chem. Soc.*, 2024, **146**, 19193–19204.

28 F. Glaser, S. De Kreijger and L. Troian-Gautier, Two Birds, One Stone: Microsecond Dark Excited-State Lifetime and Large Cage Escape Yield Afforded by an Iron–Anthracene Molecular Dyad, *J. Am. Chem. Soc.*, 2025, **147**, 8559–8567.

29 J. Toigo, K.-M. Tong, R. Farhat, S. Kamal, E. M. Nichols and M. O. Wolf, Rationalizing Photophysics of Co(III) Complexes with Pendant Pyrene Moieties, *Inorg. Chem.*, 2025, **64**, 835–844.

30 P. Dierks, A. Päpcke, O. S. Bokareva, B. Altenburger, T. Reuter, K. Heinze, O. Kühn, S. Lochbrunner and M. Bauer, Ground- and Excited-State Properties of Iron(II) Complexes Linked to Organic Chromophores, *Inorg. Chem.*, 2020, **59**, 14746–14761.

31 J. D. Braun, I. B. Lozada, C. Kolodziej, C. Burda, K. M. E. Newman, J. van Lierop, R. L. Davis and D. E. Herbert, Iron(II) Coordination Complexes with Panchromatic Absorption and Nanosecond Charge-Transfer Excited State Lifetimes, *Nat. Chem.*, 2019, **11**, 1144–1150.

32 P. Yaltseva, T. Maisuradze, A. Prescimone, S. Kupfer and O. S. Wenger, Structural Control of Metal-Centered Excited States in Cobalt(III) Complexes via Bite Angle and π–π Interactions, *J. Am. Chem. Soc.*, 2025, **147**, 29444–29456.

33 N. Sinha, B. Pfund, C. Wegeberg, A. Prescimone and O. S. Wenger, Cobalt(III) Carbene Complex with an Electronic Excited-State Structure Similar to Cyclometalated Iridium(III) Compounds, *J. Am. Chem. Soc.*, 2022, **144**, 9859–9873.

34 C. M. Brown, C. Li, V. Carta, W. Li, Z. Xu, P. H. F. Stroppa, I. D. W. Samuel, E. Zysman-Colman and M. O. Wolf, Influence of Sulfur Oxidation State and Substituents on Sulfur-Bridged Luminescent Copper(I) Complexes Showing Thermally Activated Delayed Fluorescence, *Inorg. Chem.*, 2019, **58**, 7156–7168.

35 K.-M. Tong, J. Toigo, B. O. Patrick and M. O. Wolf, Rhenium(I) Complexes with Sulfur-Bridged Dipyridyl Ligands: Structural, Photophysical, and Computational Studies, *Inorg. Chem.*, 2023, **62**, 13662–13671.

36 K.-M. Tong, J. Toigo and M. O. Wolf, Deep-Blue Phosphorescence from Platinum(II) Bis(Acetylide) Complexes with Sulfur-Bridged Dipyridyl Ligands, *Chem. Sci.*, 2025, **16**, 5948–5956.

37 C. M. Brown, M. J. Kitt, Z. Xu, D. Hean, M. B. Ezhova and M. O. Wolf, Tunable Emission of Iridium(III) Complexes Bearing Sulfur-Bridged Dipyridyl Ligands, *Inorg. Chem.*, 2017, **56**, 15110–15118.

38 C. M. Brown, T. Auvray, E. E. DeLuca, M. B. Ezhova, G. S. Hanan and M. O. Wolf, Controlling Photocatalytic Reduction of CO_2 in Ru(II)/Re(I) Dyads via Linker Oxidation State, *Chem. Commun.*, 2020, **56**, 10750–10753.

39 K. Yamamoto, W. Imai, S. Kanamori, K. Yamamoto and Y. Nakamura, Phenothiazine-, Dihydroacridine-, and Acridone-Based Boron Difluoride Complexes: Synthesis and Structure–Property Relationships, *J. Org. Chem.*, 2023, **88**, 4003–4007.

40 K. Magra, E. Domenichini, A. Francés-Monerris, C. Cebrián, M. Beley, M. Darari, M. Pastore, A. Monari, X. Assfeld, S. Haacke and P. C. Gros, Impact of the Fac/Mer Isomerism on the Excited-State Dynamics of Pyridyl-Carbene Fe(II) Complexes, *Inorg. Chem.*, 2019, **58**, 5069–5081.

41 L. M. Sigmund, F. Ebner, C. Jöst, J. Spengler, N. Gönnheimer, D. Hartmann and L. Greb, An Air-Stable, Neutral Phenothiazinyl Radical with Substantial Radical Stabilization Energy, *Chem. – Eur. J.*, 2020, **26**, 3152–3156.

42 P. Chábera, Y. Liu, O. Prakash, E. Thyrhaug, A. E. Nahhas, A. Honarfar, S. Essén, L. A. Fredin, T. C. B. Harlang, K. S. Kjær, K. Handrup, F. Ericson, H. Tatsuno, K. Morgan, J. Schnadt, L. Häggström, T. Ericsson, A. Sobkowiak, S. Lidin, P. Huang, S. Styring, J. Uhlig, J. Bendix, R. Lomoth, V. Sundström, P. Persson and K. Wärnmark, A Low-Spin Fe(III) Complex with 100 ps Ligand-to-Metal Charge Transfer Photoluminescence, *Nature*, 2017, **543**, 695–699.

43 T. A. Betley, B. A. Qian and J. C. Peters, Group VIII Coordination Chemistry of a Pincer-Type Bis(8-Quinolinyl) Amido Ligand, *Inorg. Chem.*, 2008, **47**, 11570–11582.
44 R. J. Ortiz, M. Shepit, J. van Lierop, J. Krzystek, J. Telser and D. E. Herbert, Characterization of the Ligand Field in Pseudo-Octahedral Ni(II) Complexes of Pincer-Type Amido Ligands: Magnetism, Redox Behavior, Electronic Absorption and High-Frequency and -Field EPR Spectroscopy, *Eur. J. Inorg. Chem.*, 2023, **26**, e202300446.
45 J. Zhou, L. Mao, M.-X. Wu, Z. Peng, Y. Yang, M. Zhou, X.-L. Zhao, X. Shi and H.-B. Yang, Extended Phenothiazines: Synthesis, Photophysical and Redox Properties, and Efficient Photocatalytic Oxidative Coupling of Amines, *Chem. Sci.*, 2022, **13**, 5252–5260.
46 C. A. Lucecki, N. Rani, K. K. Kpogo, J. Niklas, O. G. Poluektov, H. B. Schlegel and C. N. Verani, A New Quinoline-Based Cobalt(II) Catalyst Capable of Bifunctional Water Splitting, *Inorg. Chem. Front.*, 2025, **12**, 7411–7420.
47 C. B. Larsen, J. D. Braun, I. B. Lozada, K. Kunnus, E. Biasin, C. Kolodziej, C. Burda, A. A. Cordones, K. J. Gaffney and D. E. Herbert, Reduction of Electron Repulsion in Highly Covalent Fe-Amido Complexes Counteracts the Impact of a Weak Ligand Field on Excited-State Ordering, *J. Am. Chem. Soc.*, 2021, **143**, 20645–20656.
48 R. S. Cahn, C. Ingold and V. Prelog, Specification of Molecular Chirality, *Angew. Chem., Int. Ed.*, 1966, **5**, 385–415.
49 F. Reichenauer, C. Wang, C. Förster, P. Boden, N. Ugur, R. Báez-Cruz, J. Kalmbach, L. M. Carrella, E. Rentschler, C. Ramanan, G. Niedner-Schatteburg, M. Gerhards, M. Seitz, U. Resch-Genger and K. Heinze, Strongly Red-Emissive Molecular Ruby $[Cr(bpmp)_2]^{3+}$ Surpasses $[Ru(bpy)_3]^{2+}$, *J. Am. Chem. Soc.*, 2021, **143**, 11843–11855.
50 J.-R. Jiménez, B. Doistau, C. M. Cruz, C. Besnard, J. M. Cuerva, A. G. Campaña and C. Piguet, Chiral Molecular Ruby $[Cr(dqp)_2]^{3+}$ with Long-Lived Circularly Polarized Luminescence, *J. Am. Chem. Soc.*, 2019, **141**, 13244–13252.
51 J. D. Braun, I. B. Lozada and D. E. Herbert, In Pursuit of Panchromatic Absorption in Metal Coordination Complexes: Experimental Delineation of the HOMO Inversion Model Using Pseudo-Octahedral Complexes of Diarylamido Ligands, *Inorg. Chem.*, 2020, **59**, 17746–17757.
52 C. B. Larsen, J. D. Braun, I. B. Lozada, K. Kunnus, E. Biasin, C. Kolodziej, C. Burda, A. A. Cordones, K. J. Gaffney and D. E. Herbert, Reduction of Electron Repulsion in Highly Covalent Fe-Amido Complexes Counteracts the Impact of a Weak Ligand Field on Excited-State Ordering, *J. Am. Chem. Soc.*, 2021, **143**, 20645–20656.
53 A. Mishra, K. Sharma, C. E. Johnson, E. A. Fosu, J. Schwarz, O. Prakash, A. K. Gupta, P. Huang, F. Lindgren, L. Häggström, J. Bendix, E. Jakubikova, R. Lomoth and K. Wärnmark, Tuning the ^{2}LMCT Deactivation of Cyclometalated Iron Carbene Complexes with Electronic Substituent Effects, *Chem. – Eur. J.*, 2025, **31**, e01985.
54 O. Prakash, L. Lindh, N. Kaul, N. W. Rosemann, I. B. Losada, C. Johnson, P. Chábera, A. Ilic, J. Schwarz, A. K. Gupta, J. Uhlig, T. Ericsson, L. Häggström, P. Huang, J. Bendix, D. Strand, A. Yartsev, R. Lomoth, P. Persson and K. Wärnmark, Photophysical Integrity of the Iron(III) Scorpionate Framework in Iron(III)–NHC Complexes with Long-Lived ^{2}LMCT Excited States, *Inorg. Chem.*, 2022, **61**, 17515–17526.
55 N. Hölter, N. H. Rendel, L. Spierling, A. Kwiatkowski, R. Kleinmans, C. G. Daniliuc, O. S. Wenger and F. Glorius, Phenothiazine Sulfoxides as Active Photocatalysts for the Synthesis of γ-Lactones, *J. Am. Chem. Soc.*, 2025, **147**, 12908–12916.
56 J. A. Christensen, B. T. Phelan, S. Chaudhuri, A. Acharya, V. S. Batista and M. R. Wasielewski, Phenothiazine Radical Cation Excited States as Super-Oxidants for Energy-Demanding Reactions, *J. Am. Chem. Soc.*, 2018, **140**, 5290–5299.
57 L. Liu, T. Duchanois, T. Etienne, A. Monari, M. Beley, X. Assfeld, S. Haacke and P. C. Gros, A New Record Excited State ^{3}MLCT Lifetime for Metalorganic Iron(II) Complexes, *Phys. Chem. Chem. Phys.*, 2016, **18**, 12550–12556.
58 A. C. Bhasikuttan, M. Suzuki, S. Nakashima and T. Okada, Ultrafast Fluorescence Detection in Tris(2,2′-bipyridine) ruthenium(II) Complex in Solution: Relaxation Dynamics Involving Higher Excited States, *J. Am. Chem. Soc.*, 2002, **124**, 8398–8405.
59 N. H. Damrauer, G. Cerullo, A. Yeh, T. R. Boussie, C. V. Shank and J. K. McCusker, Femtosecond Dynamics of Excited-State Evolution in $[Ru(bpy)_3]^{2+}$, *Science*, 1997, **275**, 54–57.
60 W. Gawelda, A. Cannizzo, V.-T. Pham, F. van Mourik, C. Bressler and M. Chergui, Ultrafast Nonadiabatic Dynamics of $[Fe^{II}(bpy)_3]^{2+}$ in Solution, *J. Am. Chem. Soc.*, 2007, **129**, 8199–8206.
61 A. Lee, M. Son, M. Deegbey, M. D. Woodhouse, S. M. Hart, H. F. Beissel, P. T. Cesana, E. Jakubikova, J. K. McCusker and G. S. Schlau-Cohen, Observation of Parallel Intersystem Crossing and Charge Transfer-State Dynamics in $[Fe(bpy)_3]^{2+}$ from Ultrafast 2D Electronic Spectroscopy, *Chem. Sci.*, 2023, **14**, 13140–13150.
62 A. M. Brown, C. E. McCusker and J. K. McCusker, Spectroelectrochemical Identification of Charge-Transfer Excited States in Transition Metal-Based Polypyridyl Complexes, *Dalton Trans.*, 2014, **43**, 17635–17646.
63 M. Barra, G. S. Calabrese, M. T. Allen, R. W. Redmond, R. Sinta, A. A. Lamola, R. D. Jr. Small and J. C. Scaiano, Photophysical and Photochemical Studies of Phenothiazine and Some Derivatives: Exploratory Studies of Novel Photosensitizers for Photoresist Technology, *Chem. Mater.*, 1991, **3**, 610–616.
64 G. K. Kosgei, M. Y. Livshits, T. R. Canterbury, J. J. Rack and K. J. Brewer, Nanosecond Transient Absorption Spectroscopy of a Ru Polypyridine Phenothiazine Dyad, *Inorg. Chim. Acta*, 2017, **454**, 67–70.
65 J. Wiśniewska, G. Wrzeszcz and S. Koter, Formation of a Promazine Radical and Promazine 5-Oxide in the Reaction of Promazine with Hydrogen Peroxide: Mechanistic Insight

from Kinetic and EPR Measurements, *Int. J. Chem. Kinet.*, 2010, **42**, 1–9.

66 S. A. Kovalenko, R. Schanz, H. Hennig and N. P. Ernsting, Cooling Dynamics of an Optically Excited Molecular Probe in Solution from Femtosecond Broadband Transient Absorption Spectroscopy, *J. Chem. Phys.*, 2001, **115**, 3256–3273.

67 J. V. Caspar, E. M. Kober, B. P. Sullivan and T. J. Meyer, Application of the Energy Gap Law to the Decay of Charge-Transfer Excited States, *J. Am. Chem. Soc.*, 1982, **104**, 630–632.

68 M. E. Reinhard, B. K. Sidhu, I. B. Lozada, N. Powers-Riggs, R. J. Ortiz, H. Lim, R. Nickel, J. van Lierop, R. Alonso-Mori, M. Chollet, L. B. Gee, P. L. Kramer, T. Kroll, S. L. Raj, T. B. van Driel, A. A. Cordones, D. Sokaras, D. E. Herbert and K. J. Gaffney, Time-Resolved X-Ray Emission Spectroscopy and Synthetic High-Spin Model Complexes Resolve Ambiguities in Excited-State Assignments of Transition-Metal Chromophores: A Case Study of Fe-Amido Complexes, *J. Am. Chem. Soc.*, 2024, **146**, 17908–17916.

69 J. Wellauer, F. Ziereisen, N. Sinha, A. Prescimone, A. Velić, F. Meyer and O. S. Wenger, Iron(III) Carbene Complexes with Tunable Excited State Energies for Photoredox and Upconversion, *J. Am. Chem. Soc.*, 2024, **146**, 11299–11318.

70 J. Steube, A. Kruse, O. S. Bokareva, T. Reuter, S. Demeshko, R. Schoch, M. A. Argüello Cordero, A. Krishna, S. Hohloch, F. Meyer, K. Heinze, O. Kühn, S. Lochbrunner and M. Bauer, Janus-Type Emission from a Cyclometalated Iron (III) Complex, *Nat. Chem.*, 2023, **15**, 468–474.

71 (*a*) CCDC 2480167: Experimental Crystal Structure Determination, 2026, DOI: **10.5517/ccdc.csd.cc2p7td5**; (*b*) CCDC 2480168: Experimental Crystal Structure Determination, 2026, DOI: **10.5517/ccdc.csd.cc2p7tf6**.